Journal of Materials Processing Tech. 299 (2022) 117379

Contents lists available at ScienceDirect

Journal of Materials Processing Tech.

journal homepage: www.elsevier.com/locate/jmatprotec

Efficacy of elemental mixing of in situ alloyed Al-33wt%Cu during laser powder bed fusion

J.M. Skelton *, E.J. Sullivan, J.M. Fitz-Gerald, J.A. Floro

University of Virginia, Department of Materials Science and Engineering, Charlottesville, VA, 22903, United States

ARTICLE INFO

Associate Editor: Ian Todd

Keywords:
Laser powder bed fusion
In situ alloying
Particle size
Selective laser melting
Eutectic
Al-33wt%Cu

ABSTRACT

Challenges in developing novel alloys, specifically for use in laser powder bed fusion, may be overcome by in situ alloying of elemental powders during laser melting. This process could expedite prototyping of various alloy compositions and alleviate the restrictions and cost barriers of creating custom made alloy powder. In this research, the efficacy of in situ alloying is studied with respect to particle size distributions of the powder blends and the laser process parameters. The microstructure of the Al-Cu eutectic system is used here as an indicator of mixing quality of the constituent elements during laser melting of the particles. Hypo- or hypereutectic regions are readily visible through the dendritic growth of the α or θ phases, indicating regions where the solute concentration deviates from the nominal eutectic composition. Samples were built from four powder blends at a range of scan speeds and powers to show how mixing is affected at different processing parameters. Image analysis and Vickers microhardness tests are both used to characterize the degree of mixing within the samples. Results of this study show that poor mixing can occur due to segregation of elemental powder within the powder blend. This produces local build compositions different than the mean powder composition when the mean particle volume is large enough that the melt pool encompasses too few particles to be a stochastic representation of the blend. Liquid phase intermixing limitations within the pool are thought to be less important than the melt pool volume itself.

1. Introduction

Additive Manufacturing (AM) is an emerging technology with the potential to disrupt the current paradigm of design and engineering of metallic components. That said, there are several factors that limit the exploration of the full potential this technology has to offer. Specifically, laser powder bed fusion (LPBF) has shown potential in printing a wide variety of metal alloys, yet the quality of the built parts hinges on the type of powder feedstock used, as discussed by Vock et al. (2019). Gas atomization and plasma rotating electrode process both produce spherical powders that provide high flowability, a necessary quality for the recoating step in LPBF, but only specific alloy compositions are produced by these processes and considered commercial-off-the-shelf (COTS). Custom alloy powders can be made, but Anderson et al. (2018) bring to light several barriers of this approach, including the inability of many providers to produce small batch sizes and the high costs associated with this process. Thus, research in LPBF has been restricted and even disincentivized from exploring nonconventional alloys.

In situ alloying of powder blends within LPBF is currently being investigated as an attempt to alleviate the restrictions in acquiring unconventional powder feedstock. Several research groups have made significant progress in this area, both validating and advancing this approach. One avenue towards new alloys is to start with a conventional alloy powder, and blend in small additions of other elements. This has been performed in recent studies by Krakhmalev et al. (2017) who made small additions of Cu to Ti6Al4V to enhance the antibacterial properties of the 3D printed bio implants, and by Hanemann et al. (2019), who showed that the thermal expansion of AlSi10Mg LPBF built parts could be controlled through various additions of Si in the feedstock powder. Other studies like the those performed by Montero-Sistiaga et al. (2016) and Martin et al. (2017), attempt to modify current alloys through small additions to improve their processability through LPBF.

Beyond making minor elemental additions to pre-alloyed powder, in situ alloying is also being researched as an approach to create alloys starting entirely from elemental powder blends. This has been shown to be a viable approach for alloys with both low solute concentration such as Ti6Al4V by Simonelli et al. (2018), and high solute concentration

* Corresponding author.
E-mail address: jms3wp@virginia.edu (J.M. Skelton).

https://doi.org/10.1016/j.jmatprotec.2021.117379
Received 7 September 2021; Accepted 18 September 2021
Available online 22 September 2021

such as equiatomic NiTi shape memory alloys by C. Wang et al. (2019). Another study by P. Wang et al. (2018) used a pre-alloyed Al-4.5Cu COTS powder and combined elemental Cu powder to make Al-Cu alloys of up to 40 wt% Cu. Furthermore, a method of screening high entropy alloys has been put forth by Haase et al. (2017), and then followed by Ewald et al. (2019) where blends of over five constituent elemental powders at various compositions were alloyed in situ during LPBF. Such prototyping methods that leverage the use of low-cost elemental powders could prove to be invaluable in the development of alloys that are specifically designed to be processed by LPBF. This may be particularly important for many aluminum based alloys, where compositional changes are shown to provide solutions to many of the current processing defects that occur during LPBF as discussed in a recent review paper by Zhang et al. (2019).

Although in situ alloying during LPBF greatly expands possible alloy selections, there exist several challenges that must be better understood and overcome before this approach is widely utilized. The recent review by Mosallanejad et al. (2021) outlines six primary difference between elements within a powder blend that must be considered when performing in situ alloying, including size, melting temperature, reflectivity, viscosity, density, and thermal conductivity. Difference in melting temperatures between elemental powders is one of the most common obstacles to in situ alloying, leading to incomplete melting of one or more of the constituent elemental powders within the build. This has been observed in both the Al-Cu system by P. Wang et al. (2018) and in the Al-Si system by Roberts et al. (2016), where unmelted particles of Cu or Si were found in the bulk builds. Martinez et al. (2019), who made Al-12Cu alloys using an elemental powder blend, reported observing unmelted Cu particles and Cu rich regions within their builds, but remedied this by heating the powder bed during processing to allow for homogenization to occur. Besides having different melting temperatures, elemental particles with different size distributions may segregate in the powder hopper or recoater, leading to compositional variations within the built part. This type of dry segregation has been modeled by Yan et al. (2016) in the context of mixing that occurs within Freeman FT4 powder rheometer, showing how finer powder segregates to the bottom of the vessel during agitation. A recent review by Tan et al. (2017) discusses how similar segregation based on particle size could occur within the powder hopper of the LPBF process. The size of the elemental particles within the powder blend should also be considered with respect to the dimensions and solidification rate of the laser induced melt pool, with larger and slower melt pools allowing for higher diffusion times and greater mixing of the liquid elements.

In this study, in situ alloying of elemental Al and Cu powder is investigated with respect to the particle size distribution within the powder blend. The eutectic composition of Al-33 wt%Cu was chosen for all blends so that poor mixing of the elements in the melt pool may be observed through deviations in the eutectic microstructure. This system has been previously studied by Gill and Kurz (1993) who created a processing map showing where changes in the microstructure may be expected when varying composition and solidification rate. Regions in the melt pool that deviate from the eutectic composition by ±3 wt%Cu are shown to form either α phase (FCC Al) or θ phase (Al_2Cu) dendrites depending on whether the composition is hypo- or hypereutectic. These regions can be distinguished by both the distinct change in microstructure, as well as the difference in Z-contrast as shown through backscattered electron imaging. Using this approach, the degree of mixing in four different powder blends is analyzed with respect to the relative size distributions of the elemental powders used.

2. Method and materials

Al and Cu gas atomized powders were purchased from Valimet Inc. (Cu-1, Al-1, and Al-2 as shown in Table 1) and Thermo Scientific (Cu-2) at four different size distributions. A pre-alloyed Al-33 wt%Cu powder, also obtained from Valimet, was used as a control, providing the best-case scenario of mixing in built samples. The elemental feedstock powders were characterized using an FEI Quanta 650 field emission scanning electron microscope (SEM) and the composition of the elemental particles were confirmed using energy-dispersive X-ray spectroscopy (EDS). Size distributions were calculated using ImageJ software to detect and measure the areas of the particles within the micrographs. Over 3,000 particles from each of the four elemental feedstock powders were imaged and measured, in accordance with studies performed by Mazzoli and Favoni (2012) and Igathinathane et al. (2008) that used this same particle analysis approach. Feedstock powders were then combined in four different binary blends, with both Al and Cu powder being weighed out at the eutectic ratio, and then mechanically mixed for two hours. Dry mixing was performed within a stainless-steel container using a SPEX 8000 M mill in ambient atmosphere and pressure. No balls were used during the mixing process to avoid deformation of the powder. Table 1 shows the four different blends of powders and the d_{50} of the elemental feedstock powders. Rheology data of the powder blends was obtained from a Freeman FT4 powder rheometer directly after drying under Ar for over 24 h to reduce humidity.

Table 1
All four combinations of the elemental feed stock powder, where each blend made Al-33 wt%Cu.

Elemental Powder (d_{50})	Cu-1 (2 μm)	Cu-2 (6 μm)
Al-1 (9 μm)	Blend 1	Blend 2
Al-2 (30 μm)	Blend 3	Blend 4

Samples were processed with a SLM 125 from SLM Solutions GmbH. A manual recoating method was used instead of the traditional automated set up to decrease the required quantity of the powder blend. To perform the manual recoating, an aluminum container with approximately 1 mm holes on the bottom was used to evenly disperse powder blends onto the build substrate via sifting. A stainless-steel straight edge was then used to remove any excess powder, ensuring a powder layer thickness as controlled by the precise lowering of the build plate. Following the manual powder coating, laser melting was performed and the recoating process was repeated. Samples were made using each of the four powder blends at six different laser parameters as shown in Table 2. The hatch spacing remained constant for all builds at 100 μm, as did the powder layer thickness (50 μm), and laser beam width (100 μm). The dimensions of the samples made were approximately 5 mm x 5 mm and approximately 2.5 mm in the build direction (typical around 50 layers). The build plate used for these samples was a 6061-aluminum alloy, 12.7 mm thick plate that was later cross-sectioned with the samples. Dilution from the base plate was observed in all samples to some degree, particularly evident in samples processed at higher laser powers. However, the dilution was confined to the first ten layers of the build. Samples were cut longitudinally (in the scan direction) while still attached to the base plate using a Mager BR220 precision cut-off saw. These samples were then ground and polished down to a 0.05 μm finish using a silica colloidal suspension. The microstructure and composition of these samples were analyzed using backscattered electron imaging (BSI) and EDS within the SEM. Micrographs were post-processed and analyzed using ImageJ software to quantify areas of hypo or hypereutectic microstructures within the samples. Vickers microhardness measurements of built samples were taken using a Wilson VH1150 using an HV (0.2) and a dwell time of 5 s.

Table 2
Different parameters used to process elemental powder blends.

	50 mm/s	100 mm/s	200 mm/s	300 mm/s
125 W		AM4		
150 W	AM1	AM3	AM5	AM6
200 W		AM2		

3. Results and discussion

3.1. Powder characterization

Elemental powder feedstock was characterized to observe sphericity of particles as well as to obtain particle size distribution. Fig. 1 shows the micrographs of the four elemental powders and their size distributions as calculated using ImageJ software. The larger Al powder (Al-2) was specifically developed for use in LBPF by Valimet and was found to have the narrowest particle size distribution as observed in Fig. 1**e**. The four combinations of these elemental powders resulting in the four powder blends are shown in Fig. 2. In blends 1 and 3 (Fig. 2) the smaller Cu powder (Cu-1) was found to be embedded on the surface of the Al particles after mechanical mixing, most likely due to inter-particle impacts or static charge effects. Although blend 3 appears to have a higher coverage of Cu particles on the larger Al particles than in blend 1, the actual wt% of adhered Cu particles is greater in blend 1. In blends 2 and 4 (Fig. 2**)** no adherence was observed between the Al and Cu particles. These inherent differences in the powder blends lead to differences in the overall elemental distributions within a powder layer during the LPBF process, as will be further discussed in subsequent sections. Characterization of the powders were performed using EDS to ensure that no impurities had contaminated the powder during mechanical mixing (see supplemental material Figure S-1).

Rheology data obtained from the Freeman FT4 rheometer allowed for comparison of powder blends through several different properties. Fig. 3**a** shows the compressibility of the blends, which can be used as an indicator of powder flowability, although this property alone cannot predict how well the powder will flow during the recoating process in LPBF as discussed in a review of granular flow properties by Schwedes (2003). The shear stress of the powder blends (Fig. 3d) provides a metric that is more comparable with the motion of the particle sliding under the recoater blade, which places the powder both in shear and uniaxial compression. From the shear stress tests, several other properties can also be extracted to characterize the powder. The powder property that most correlates with the flowability is the unitless flow function (FF), which is derived from the ratio of the major principle stress (MPS) and the unconfined yield strength (UYS). Powders with an FF < 1 are considered non-flowing while those with an FF > 10 are considered free flowing as described by Søgaard et al. (2012). The difference between the Al-2 (30 μm) elemental powder designed specifically for LPBF and the four powder blends can be clearly seen within this property, with the former having FF $= 10.2$ and the latter having FF $= 3.8$–5.4, as shown in Fig. 3**c.** The reason for the decrease in flowability of the powder blends may be attributed to both the strongly bimodal particle size distributions of the blends as well as a decrease in the average sphericity of the gas atomized Cu powders, especially Cu-2 (6 μm), which was found to have many irregularly shaped particles. Blends of smaller powder sizes are also more prone to absorb moisture when testing in air due to their abundance of surface area, and therefore may flow better within an inert environment then indicated by the rheometry data.

The flowability of the feedstock powder in LPBF has far reaching consequences, thus maximizing this property when designing elemental powder should be a priority that is balanced with other desirable attributes such as a homogenous distribution of the elemental powder, and particle sizes that allow for elemental mixing to occur within the melt pool. The powder blends studied in this investigation represent the lower size range of feedstock powder that could feasibly be used in LBPF due to their low flowability, yet trends from the different combinations of size ratios and insight into elemental blend design will be applicable to larger, and possibly more spherical, powder feedstock.

3.2. Microstructure analysis

Characterization of the samples built from the different elemental powder blends allowed for a qualitative comparison of the elemental mixing achieved during laser melting. Samples made from a pre-alloyed powder were used to allow for a comparison of the microstructures. Fig. 4 shows the microstructures of samples made from the four powder blends processed at the AM5 laser parameter (Table 2).

EDS performed on the dark and bright regions of the BSE micrographs confirm that these regions correspond to higher concentrations of Al and Cu respectively, as shown in Fig. 5a–c. Due to the nature of eutectic solidification, deviations from the Al-33 wt%Cu composition in the melt pool result in local changes to the nominal lamellar microstructure, where either α-phase or θ-phase dendrites will begin to form, depending on the shift in composition. Fig. 5d and e show micrographs of the hyper- and hypoeutectic regions, where θ-phase and α-phase dendrites are present. It should be noted here that some areas that are high in Cu concentration from the EDS maps, and that appear bright in backscatter micrographs, actually still retain the nominal lamellar microstructure. These areas are usually found close to θ-phase dendrites, and may result from an extension of the hypereutectic region under the surface that is being detected by the interaction volume of both the backscattered electrons and characteristic x-rays. Similarly, dark areas are also seen around many of the α dendrites. Such regions were categorized as part of the overall hyper- or hypoeutectic region, even though there exist no change in the microstructure.

To quantify the degree of mixing, regions of high or low Z-contrast in the BSE micrographs were measured through ImageJ software. An example of the selection process for a hypereutectic region is shown in Fig. 6, where thresholding is used to select pixels above a certain

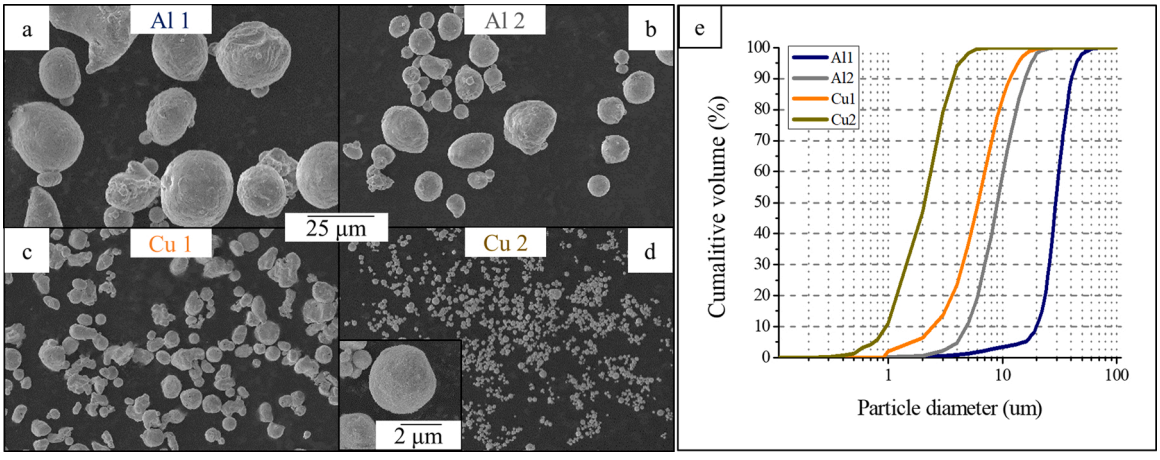

Fig. 1. SEM micrographs of elemental powder feedstock of Al (a and b) and Cu (c and d) with corresponding particle size distributions taken from areas of particles calculated in ImageJ (e). In set in (d) shows morphology of Cu2 particles. Micrographs (a-d) are all scaled to the center scale bar.

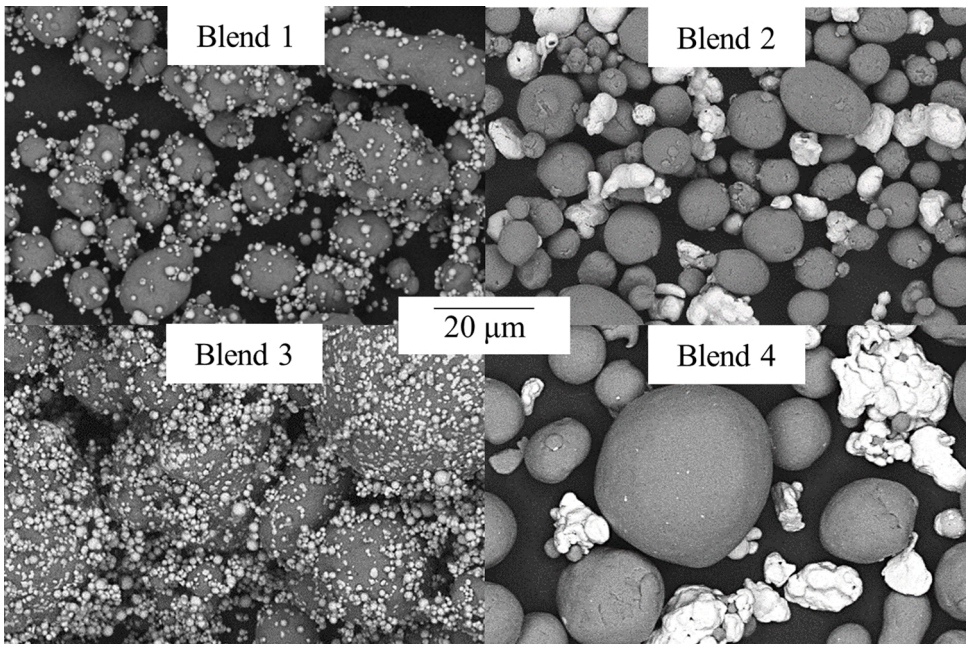

Fig. 2. Four elemental powder blends of various sizes of Al and Cu powder mixed at the eutectic composition. SEM micrographs were taken after blends were mechanically mixed for 2 h. The lighter-contrast particles are Cu while the darker particles are Al. All micrographs are scaled to the same scale bar.

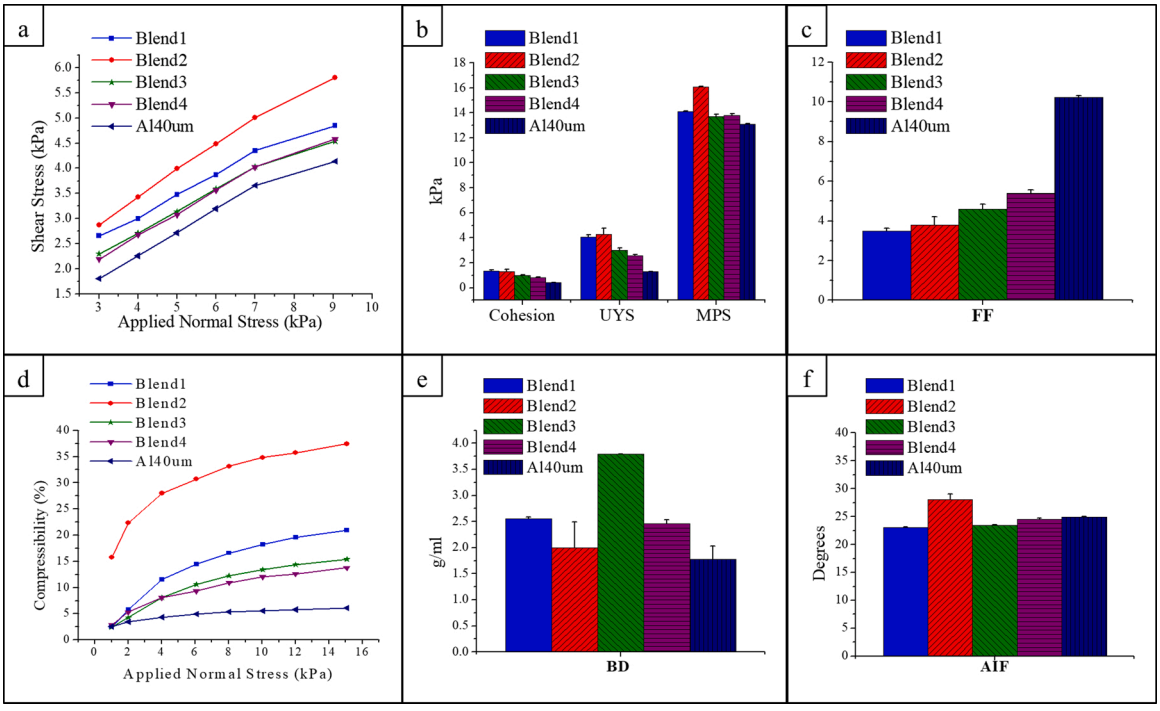

Fig. 3. Rheology data of powder blends showing the compressibility (a) and the shear stress (d) of the powder. From the shear stress data, several other powder properties may be gained such as the cohesion, unconfined yield strength (UYS), major principal stress (MPS) (b), flow function (FF) (c), bulk density (BD) (e), and angle of internal friction (AIF) (f). The Al (30 μm) elemental powder is plotted with the blends for comparison.

greyscale level and the selected area is then measured. Because these samples were built layer-by-layer through LPBF, coarsening of the microstructure occurs at the melt pool boundaries, and these are assigned by the software as part of the hyper- or hypoeutectic regions as seen in the numerous fine-scale lines across the background of Fig. 6b. To eliminate this, a minimum area filter was used during the particle analysis process (Fig. 6c). An average of three SEM micrographs per sample were analyzed giving a total of 72 (3 micrographs x 6 parameters x 4 blends) images that were processed to quantify both the hyper- and hypoeutectic regions.

Trends in the percentage of hyper- and hypoeutectic areas in samples processed with the different powder blends at increasing powers can be seen in Fig. 7. Blend 4 had the highest percentages of hyper- and hypoeutectic areas, which implies the lowest degree of in situ mixing for this blend. However, mixing of blend 4 improved markedly with increasing power. In general, the results from the different blends tend

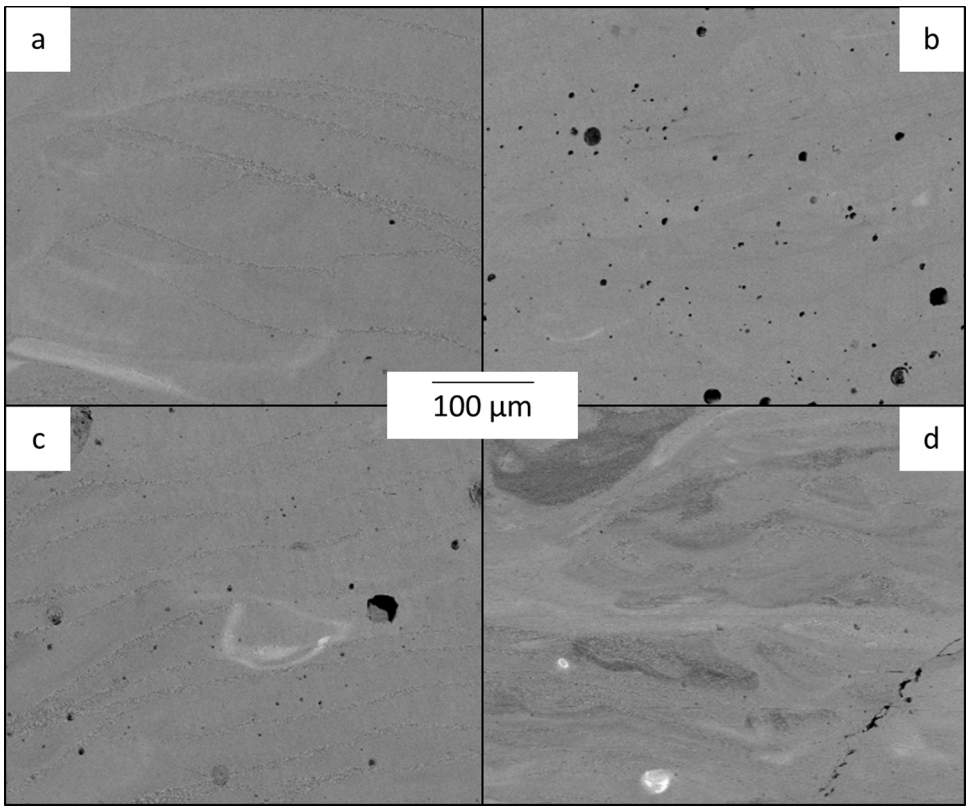

Fig. 4. SEM Backscattered micrographs of microstructures of samples built from the powder blends 1(a), 2(b), 3(c), and 4(d) all processed at AM5. Bright regions indicate region of high Cu concentration (hypereutectic) while darker gray regions indicate locally elevated Al concentrations (hypoeutectic). Black spots in micrographs are spherical pores. All micrographs are scaled to the same scale bar.

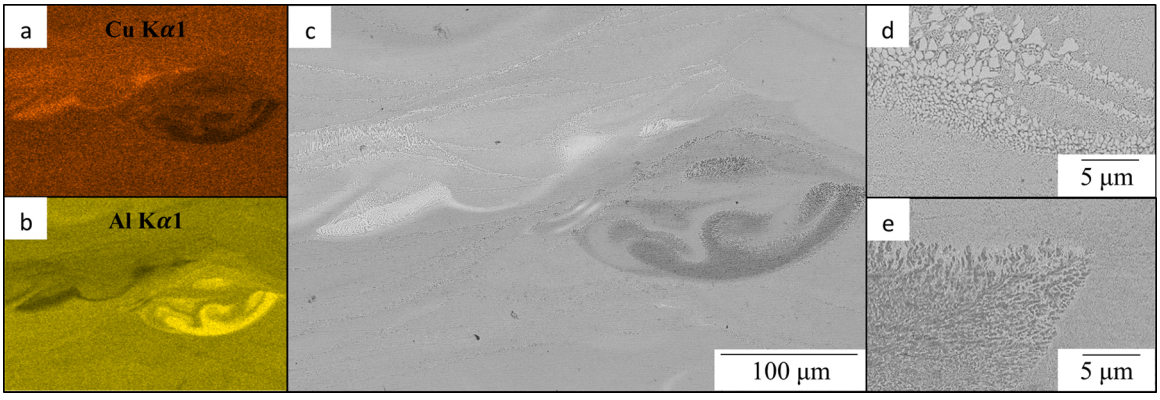

Fig. 5. SEM EDS maps of Cu (a) and Al (b) in a sample made from blend 4 at the AM1 laser parameter. Light and dark regions in the backscattered micrograph (c) correspond to high concentrations of Cu or Al respectively. Higher magnification micrographs of the Cu and Al rich regions are shown to have hypereutectic (d) and hypoeutectic (e) microstructures.

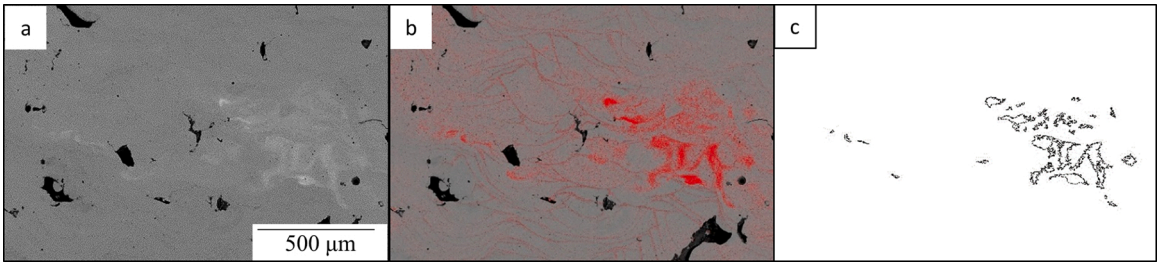

Fig. 6. Example of a hypereutectic region in a BSE micrograph (a) being selected through thresholding (b) and then quantified using ImageJ (c).

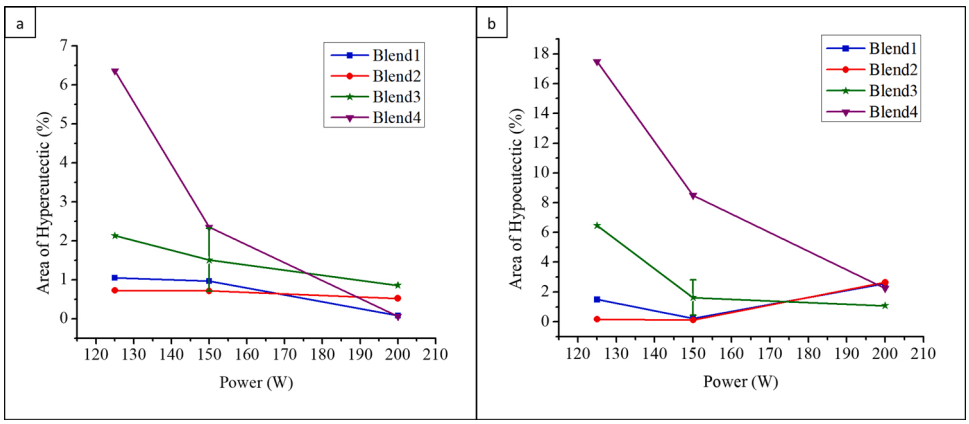

Fig. 7. Quantification of hypereutectic (a) and hypoeutectic (b) areas in samples processed from the different powder blends at increasing powers. Error bars were placed on one of the data points (blend 3, 150 W) to show an approximate range of uncertainty of this analysis based on thresholding variability.

to converge at the higher powers. At 200 W, the area percentages of the hypereutectic regions were from 0 to 1 %, while the hypoeutectic regions converged in the range of 1–3 %. Fig. 7b shows that samples made from blends 1 and 2 appear to exhibit worse mixing a laser power of 200 W vs. 150 W. Keyholing was observed to occur in the samples when processed at 200 W, forming a deep melt pool that results in more intermixing with the aluminum base plate. In blends 1 and 2 this effect is more evident since good mixing was already occurring at lower powers. This also explains why such a trend is not observed in the percentage of hypereutectic regions in the same samples.

The stronger dependence of mixing with increasing laser power observed in blend 4 may be explained in part by the larger powder sizes. Coarser particle size requires larger melt pools to envelop a statistically representative number of particles, in order to achieve the average liquid composition that is on or near the eutectic. This requires a very thorough mixing of the elemental powders, and is facilitated by use of smaller powder diameters. In particular, when the melt pool dimension is only a factor larger than the mean particle size, severe local fluctuations in the local blend composition are likely. Additionally, a smaller powder diameter size also reduces the diffusion distance between alloy components within the laser melt pool. Lee and Cahoon provided experimental data showing the interdiffusion coefficient of copper in liquid aluminum to be 8.39×10^{-9} m^2/s, implying a solute atoms diffusion length of approximately 4 μm in a 200 μm melt pool, assuming a laser scan velocity of 100 mm/s (Lee and Cahoon, 2011). However, the length scale of mixing is unlikely to be dictated solely by diffusion due to convective and Marangoni currents within the melt pool. Nonetheless, the size of the particles will play a role in mixing efficacy within the transient liquid, especially as the size of the melt pool decreases at lower laser powers. Taken together, these considerations show that even small degrees of powder segregation within powder blends that use larger particles (>30 μm) will adversely affect the in situ alloying much more than in blends with a smaller average powder size. A large degree of chemical segregation of the elemental powders within the powder layer, i.e. groupings of either Al-Al or Cu-Cu particles greater than approximately 100 μm in diameter, can cause the composition of the melt pool to diverge from the average composition, producing local hypo- or hypereutectic regions. Coarser powders (> 30 μm) are more prone to statistical fluctuations in local powder composition in this size range due to the fact that fewer particles are needed in a group to reach these dimensions, as observed with blend 4. Furthermore, two types of mixing may occur due to the differences in sizes of the elemental powder – one is the standard mixing of the independent powder particles, while the other type of mixing is via mechanical embedding, wherein minority (by weight) Cu particles are joined to the majority Al particles by mutual impact to form Hertzian contacts. The more this latter type of mixing occurs, the less likely it is that large amounts of free powder segregation can occur. Mechanical embedding will be less effective for larger Al particles as these have a lower surface area to volume ratio, and as such will allow fewer relatively smaller particles (2 um Cu) to be embedded on their surface. A rough estimate of the wt% of Cu particles that were embedded on the surface of the 30 μm Al powder was made through the following equation:

$$wt\%\ Cu = \frac{N_{Cu} V_{Cu} \rho_{Cu}}{V_{Al} \rho_{Al}} = 4 C_{Cu} \left(\frac{\bar{r}_{Cu} \rho_{Cu}}{\bar{r}_{Al} \rho_{Al}} \right) \quad (1)$$

Equation 1 takes the total mass of the surface embedded Cu to be the number of embedded Cu particles, N_{Cu}, times the volume of each times the density, ρ_{Cu}, and normalizes this by the mass of the Al particle. The final expression makes the simplifying assumption that Cu particles of the mean size in the original powder are embedded at constant mass into an Al particle of the mean size. The final expression contains C_{Cu}, which is the average areal fraction of Cu particles on the larger Al particles. By analyzing micrographs of blend 3 with ImageJ software, the average areal coverage of the Cu (2 μm) particles on the Al (30 μm) particles was found to be 14 % (see supplemental material Figure S-2). These embedded Cu particles were estimated to be hemispheres since only the flat surface of the particles could be seen. Thus, the average composition of Cu embedded in the Al particles in blend 3 was found to be 12.2 wt%. This suggests that a large amount of the Cu (2 μm) was free within the elemental blend to agglomerate. In contrast, the smaller Al (9 μm) powder used in blend 1 contained much more surface area for the Cu (2 μm) particles to adhere to. As such, even though only 9% of the surface area of the Al (9 μm) particles were covered with Cu particles, this amounted to 26.6 wt%Cu, suggesting that much less of the Cu (2 μm) particles were available to agglomerate within the blend. When regarding the liquid mixing occurring during laser melting of blends 1 and 3, the Cu not embedded into the larger Al particles may tend to agglomerate within the blends, leading to regions of both hyper- and hypoeutectic compositions within the melt pool which may not fully homogenize before solidification. Because it was shown that blend 3 has a smaller wt% of embedded Cu particles than blend 1, it is likely that this is the cause of increased hypo- and hypereutectic regions within samples made from blend 3 (Fig. 7).

It should be noted here that the manual recoating used in this study may provide results that differ slightly from autonomous builds in terms of creating an even distribution of the elemental powders in each layer. Yet the manual recoating method should provide optimum results for two reasons. First, the application of the powder blends in the manual recoating process greatly reduces powder transport distance, allowing less opportunity for elemental particles to segregate based on density, while the autonomous method requires the powder to travel through several feet of tubing from the hopper to the recoater. Second, the manual recoating method allows for visual inspection of each powder

layer applied to the build, ensuring that large gaps in the powder layer may be detected and remedied by a repeated application and leveling of the powder blend. Thus, if elemental segregation occurs in samples built through the manual recoating method, it is very likely that similar or worse results will be found in samples built through the autonomous recoating method.

3.3. Analysis of mixing through hardness measurements

Vickers microhardness measurements were used as a complementary characterization method to evaluate the local variations of the mechanical properties across a sample. In the Al-Cu system, the tetragonal θ-phase is harder than the FCC α-phase. In the two-phase eutectic lamellar microstructure, hardness will increase as the spacing between the phases decreases. Thus, the coarse α dendrites of the hypoeutectic regions will give a lower hardness value then the fine lamellar microstructure of the eutectic composition, due to both the length scales of the microstructure as well as the lack of the θ-phase present. In regions of the sample that are hypereutectic, it can be expected that the hardness value will be equal to or greater than the surrounding eutectic microstructure. The average diameter for an HV (0.2) indent in these samples was approximately 50 μm, which in principle would provide a high enough spatial resolution to detect hyper- or hypoeutectic regions with areas on the order of 100 μm^2 (Fig. 4). Because coarsening occurs at the melt pool boundaries, the hardness was found to decrease by ~50 HV (0.2) when the indenter was centered on these features. Measurements were thus taken in between these boundaries whenever possible.

Fig. 8 shows the average hardness values for each sample processed from the four different powder blends with their associated error. The average hardness values of samples built from a pre-alloyed powder are also shown (in black) for comparison. Because the solidification of the microstructure occurs at different rates from the bottom of the melt pool to the top due to the curvature of the solidification front, the interlamellar spacing becomes finer near the surface of the melt pool, and thus the hardness can be expected to increase with the finer microstructure. Lei et al. (2017) measured this variation of hardness to be on the order 1 GPa within a laser melted Al-Cu eutectic sample through the use of a nanoindenter. The variance in hardness seen in the samples made from the pre-alloyed powder, which contained no hyper- or hypoeutectic regions, was found to be approximately 50 HV (~490 MPa), which may be the result of the using a microindenter in this study rather than a nanoindenter.

Variations in hardness between the pre-alloyed samples are largely attributed to the different laser velocities used within this parameter set. Higher laser velocities cause higher solidification rates within the melt pool which decreases the lamellar spacing. This refinement of the lamellar spacing occurs up to a peak hardness at 200 mm/s, after which increases in the laser velocity cause the lamellar microstructure to transition into a fine dendritic like microstructure as shown by Gill and Kurz (1993). These changes in the microstructure caused by varying laser velocity are most prominent near the surface of the melt pool, where the solidification rate is nearer to the laser velocity, but diminished lower in the melt pools due to the dependence of the solidification rate on the curvature of the solid-liquid interface as discussed earlier. Thus, difference in hardness between samples depends on where the microhardness test was taken within the melt pool. Even so, a trend can be seen between the pre-alloyed samples, with AM1 (50 mm/s, 150 W), AM3 (100 mm/s, 150 W) and AM5 (200 mm/s, 150 W) having increasingly hard microstructures, while AM6 (300 mm/s 150 W) decreases in hardness, most likely due to the transition from the fine eutectic to a fine dendritic microstructure.

The best correspondence of the hardness values between the samples

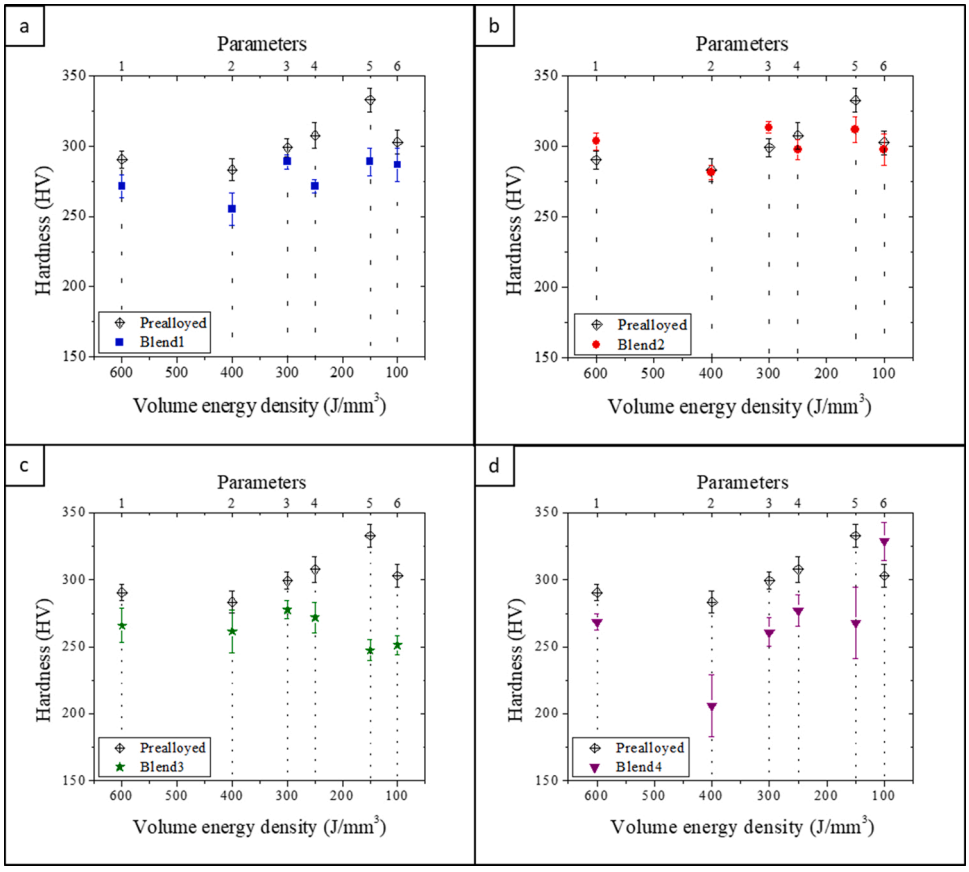

Fig. 8. Hardness distributions of samples processed at the six laser parameters for powder blends 1-4 (a-d). Hardness values for samples built from the pre-alloyed powder are overlaid on all graphs for comparison. Parameters are arranged from highest to lowest volume energy density (J/mm^3).

made from the pre-alloyed powder and the samples formed by in situ alloying can be found in blend 2, while the worst overlap, and widest hardness ranges, are found in blend 4. This trend in the data correlates with trends in the structural inhomogeneity determined from image analysis of the hyper- and hypoeutectic regions (Fig. 7). All powder blends show a relatively good correlation to the hardness of the pre-alloyed powder at the processing parameter with the highest energy density (AM1) and that this correlation worsens in parameters with lower energy density, specifically in blends 3 and 4.

The porosity of these samples should also be taken into consideration, both when considering the hardness values, as well as in terms of the overall processability of the powder. The relationship of the hardness and the porosity of the samples appears to not be directly correlated, as the samples made from blend 4 showed the widest range of hardness values, while in Fig. 9 it is shown to have the least amount of porosity for the majority of the parameters. Blend 2 in contrast had some of the smallest ranges of hardness values, while having some of the highest porosity of the blends. In regards to the processability of the powder, it is difficult to discern any clear trends relating to the porosity of the bulk samples and the size of the powder blends they were built from. A few distinctions may be made between the blends though, such as blend 4 appears to have the lowest porosity across the parameter range. This could perhaps be related to the flowability of blend 4, as less clumping within the powder layer could produce a denser part. The higher energy density parameter (AM1) appears to produce samples with the lowest porosity for all four blends, although blend 4 trends to even lower porosity at lower energy density parameters. Trends may also be obscured by the different types of porosity that are occurring. For example, lack of fusion pores may be the cause of high porosity at lower energy densities, while keyholing porosity may be present at higher energy densities. Further fine tuning of the processing parameters may yield more fully dense samples for each of these powder blends, with such features as hatch spacing or laser spot size that could be adjusted to decrease lack of fusion porosity within the builds.

4. Conclusion

The in situ alloying of Al-33 wt%Cu was studied in order to determine the effect powder feedstock size and processing parameters have on the mixing of the elemental powders during LPBF. The solidification microstructure of this eutectic alloy was used to assess the degree of mixing that occurred within each sample. This was performed both quantitatively through the use of SEM and image analysis and qualitatively through the use of Vickers microhardness testing. Significant results are summarized through the following:

1 Measurements of local compositional fluctuations within an Al-Cu eutectic alloy processed through LPBF in situ alloying have been performed using the eutectic microstructure as an indicator of variations of the solute concentration of up to a few weight percent. This system allowed for both the size and location of compositional fluctuations to be readily observed, and provided a method to quantify what percentage of the sample was off the desired composition with the use of image analysis software
2 The particle size distribution of the blends was shown to be directly correlated with the degree of compositional homogeneity that existed in the built samples across a range of processing parameters. Particle sizes that are customary to the LPBF processing method were shown to produce large regions of compositional fluctuations, while powder blends with smaller size distributions produced samples with only small regions of compositional fluctuations.
3 Particle decoration in powder blends was studied in an attempt to reduce dry segregation of elemental powder, with limited success, due to the large amount of solute concentrations in this alloy. Small Cu powder (2 μm) that did not adhere to the larger Al particles readily clumped, and were most likely the cause of hypereutectic regions within blends 1 and 3.

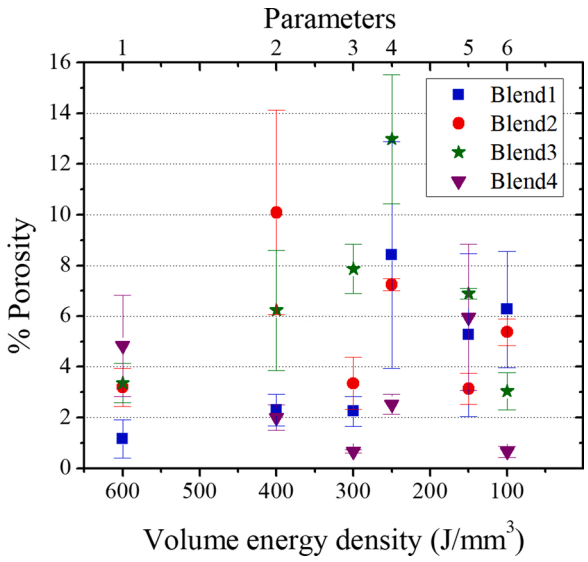

Fig. 9. Porosity of samples built from all four elemental powder blends. Measurements were made by calculating the area fraction of porosity in cross-sections of each sample as observed through SEM characterization. The average of three measurements per sample are shown along with the corresponding error bars.

These results help lay the groundwork for a rational design of elemental powder blends that optimizes mixing during in situ alloying within a given set of laser parameters.

Declaration of Competing Interest

The authors declare the following financial interests/personal relationships which may be considered as potential competing interests:

Acknowledgements

Support from the National Science Foundation under award NSF-1663085 is gratefully acknowledged. Utilization of the FEI LV650 SEM and FEI Helios G4 DualBeam within UVa's Nanoscale Materials Characterization Facility (NMCF) was crucial to this work. A sincere thank you to Prof. Tao Sun and Prof. Ji Ma and their respective groups at UVA for the use of their lab space and equipment.

Appendix A. Supplementary data

Supplementary material related to this article can be found, in the online version, at doi:https://doi.org/10.1016/j.jmatprotec.2021.117379.

References

Anderson, I.E., White, E.M.H., Dehoff, R., 2018. Feedstock powder processing research needs for additive manufacturing development. Curr. Opin. Solid State Mater. Sci. https://doi.org/10.1016/j.cossms.2018.01.002.

Ewald, S., Kies, F., Hermsen, S., Voshage, M., Haase, C., Schleifenbaum, J.H., 2019. Rapid alloy development of extremely high-alloyed metals using powder blends in laser powder bed fusion. Materials (Basel). 12, 1–15. https://doi.org/10.3390/MA12101706.

Gill, S.C., Kurz, W., 1993. Rapidly solidified AlCu alloys-I. experimental determination of the microstructure selection map. Acta Metall. Mater. 41, 3563–3573. https://doi.org/10.1016/0956-7151(93)90237-M.

Haase, C., Tang, F., Wilms, M.B., Weisheit, A., Hallstedt, B., 2017. Combining thermodynamic modeling and 3D printing of elemental powder blends for high-throughput investigation of high-entropy alloys – towards rapid alloy screening and

design. Mater. Sci. Eng. A 688, 180–189. https://doi.org/10.1016/j.msea.2017.01.099.
Hanemann, T., Carter, L.N., Habschied, M., Adkins, N.J.E., 2019. In-situ alloying of AlSi10Mg + Si using selective laser melting to control the coefficient of thermal expansion. J. Alloys. Compd. 795, 8–18.
Igathinathane, C., Pordesimo, L.O., Columbus, E.P., Batchelor, W.D., Methuku, S.R., 2008. Shape identification and particles size distribution from basic shape parameters using ImageJ. Comput. Electron. Agric. 63, 168–182. https://doi.org/10.1016/j.compag.2008.02.007.
Krakhmalev, P., Yadroitsev, I., Yadroitsava, I., de Smidt, O., 2017. Functionalization of biomedical Ti6Al4V via in situ alloying by Cu during laser powder bed fusion manufacturing. Materials (Basel) 10. https://doi.org/10.3390/ma10101154.
Lee, N., Cahoon, J., 2011. Interdiffusion of copper and iron in liquid aluminum. J. Phase Equilibria Diffus. 32, 226–234. https://doi.org/10.1007/s11669-011-9883-0.
Lei, Q., Ramakrishnan, B.P., Wang, S., Wang, Y., Mazumder, J., Misra, A., 2017. Structural refinement and nanomechanical response of laser remelted Al-Al2Cu lamellar eutectic. Mater. Sci. Eng. A 706, 115–125. https://doi.org/10.1016/j.msea.2017.08.105.
Martin, J.H., Yahata, D., Hundley, J.M., Mayer, J.A., Schaedler, T.A., Pollock, T.M., 2017. 3D printing of high-strength aluminium alloys. Nature 549, 365–369. https://doi.org/10.1038/nature23894.
Martinez, R., Todd, I., Mumtaz, K., 2019. In situ alloying of elemental Al-Cu12 feedstock using selective laser melting. Virtual Phys. Prototyp. 14, 242–252. https://doi.org/10.1080/17452759.2019.1584402.
Mazzoli, A., Favoni, O., 2012. Particle size, size distribution and morphological evaluation of airborne dust particles of diverse woods by Scanning Electron Microscopy and image processing program. Powder Technol. 225, 65–71. https://doi.org/10.1016/j.powtec.2012.03.033.
Mosallanejad, M.H., Niroumand, B., Aversa, A., Saboori, A., 2021. In-situ alloying in laser-based additive manufacturing processes: a critical review. J. Alloys. Compd. 872, 159567 https://doi.org/10.1016/j.jallcom.2021.159567.
Roberts, C.E., Bourell, D., Watt, T., Cohen, J., 2016. A novel processing approach for additive manufacturing of commercial aluminum alloys. Phys. Procedia 83, 909–917. https://doi.org/10.1016/j.phpro.2016.08.095.
Schwedes, J., 2003. Review on testers for measuring flow properties of bulk solids. Granul. Matter 5, 1–43. https://doi.org/10.1007/s10035-002-0124-4.
Simonelli, M., Aboulkhair, N.T., Cohen, P., Murray, J.W., Clare, A.T., Tuck, C., Hague, R. J.M., 2018. A comparison of Ti-6Al-4V in-situ alloying in Selective Laser Melting using simply-mixed and satellited powder blend feedstocks. Mater. Charact. 143, 118–126. https://doi.org/10.1016/J.MATCHAR.2018.05.039.
Montero-Sistiaga, M.L., Mertens, R., Vrancken, B., Wang, X., Van Hooreweder, B., Kruth, J.P., Van Humbeeck, J., 2016. Changing the alloy composition of Al7075 for better processability by selective laser melting. J. Mater. Process. Technol. 238, 437–445. https://doi.org/10.1016/j.jmatprotec.2016.08.003.
Søgaard, S., Bryder, M., Allesø, M., Rantanen, J., 2012. Characterization of powder properties using a powder rheometer. Proc. Electron. Conf. Pharm. Sci. https://doi.org/10.3390/ecps2012-00825, 2.
Tan, J.H., Wong, W.L.E., Dalgarno, K.W., 2017. An overview of powder granulometry on feedstock and part performance in the selective laser melting process. Addit. Manuf. 18, 228–255. https://doi.org/10.1016/j.addma.2017.10.011.
Vock, S., Klöden, B., Kirchner, A., Weißgärber, T., Kieback, B., 2019. Powders for powder bed fusion: a review. Prog. Addit. Manuf. 4, 383–397. https://doi.org/10.1007/s40964-019-00078-6.
Wang, P., Deng, L., Prashanth, K.G., Pauly, S., Eckert, J., Scudino, S., 2018. Microstructure and mechanical properties of Al-Cu alloys fabricated by selective laser melting of powder mixtures. J. Alloys. Compd. 735, 2263–2266. https://doi.org/10.1016/J.JALLCOM.2017.10.168.
Wang, C., Tan, X.P., Du, Z., Chandra, S., Sun, Z., Lim, C.W.J., Tor, S.B., Lim, C.S., Wong, C.H., 2019. Additive manufacturing of NiTi shape memory alloys using pre-mixed powders. J. Mater. Process. Technol. 271, 152–161. https://doi.org/10.1016/j.jmatprotec.2019.03.025.
Yan, Z., Wilkinson, S.K., Stitt, E.H., Marigo, M., 2016. Investigating mixing and segregation using discrete element modelling (DEM) in the Freeman FT4 rheometer. Int. J. Pharm. 513, 38–48. https://doi.org/10.1016/j.ijpharm.2016.08.065.
Zhang, J., Song, B., Wei, Q., Bourell, D., Shi, Y., 2019. A review of selective laser melting of aluminum alloys: processing, microstructure, property and developing trends. J. Mater. Sci. Technol. 35, 270–284. https://doi.org/10.1016/j.jmst.2018.09.004.